Weld Metal Composition Change during Conduction Mode Laser Welding of Aluminum Alloy 5182

H. ZHAO and T. DEBROY

Selective vaporization of volatile elements during laser welding of automotive aluminum alloys affects weld metal composition and properties. An experimental and theoretical study was carried out to seek a quantitative understanding of the influences of various welding variables on vaporization and composition change during conduction mode laser welding of aluminum alloy 5182. A comprehensive model for the calculation of vaporization rate and weld metal composition change was developed based on the principles of transport phenomena, kinetics, and thermodynamics. The calculations showed that the vaporization was concentrated in a small high-temperature region under the laser beam where the local vapor pressure exceeded the ambient pressure. The convective vapor flux driven by the pressure gradient was much higher than the diffusive vapor flux driven by the concentration gradient. The computed weld pool geometry, vaporization rates, and composition changes for different welding conditions agreed well with the corresponding experimental data. The good agreement demonstrates that the comprehensive model can serve as a basis for the quantitative understanding of the influences of various welding variables on the heat transfer, fluid flow, and vaporization occurring during conduction mode laser welding of automotive aluminum alloys.

I. INTRODUCTION

THE 2000, 5000, and 6000 series aluminum alloys chosen for automotive applications provide substantial specific strength, good crash-worthiness, and excellent corrosion resistance.[1] Laser beam welding is characterized by high welding speed, low heat input, and low weldment distortion; it is also amenable to automation. These attributes make laser beam welding potentially attractive for the joining of automotive components in drive train assemblies, suspension components, and various body panels.[2,3] Currently, however, hot cracking, porosity, and weld metal composition change are major concerns in the welding of aluminum alloys for automotive applications.[4]

Weld metal composition change caused by selective vaporization of volatile alloying elements, especially magnesium, may affect the mechanical properties, corrosion resistance, and hot crack susceptibility of the weldment.[5,6,7] The yield strength of 5000 series aluminum alloys increases linearly with the concentration of magnesium, as shown in Figure 1.[5] Loss of magnesium results in loss of the yield strength of these alloys. Cieslak and Fuerschbach[6] investigated the loss of hardness resulting from the laser welding of aluminum alloys. They found that magnesium vaporization from the weld pool results in reduced weld metal hardness as compared with an equivalently treated base metal. For the alloys 5456 and 5086, they proposed that the loss of hardness resulted from a diminished solid solution strengthening effect caused by a lower magnesium concentration. The compositional and microstructural changes across the weldment may also deteriorate the corrosion resistance of the alloy.[5] Finally, it is known that the hot crack susceptibility of aluminum alloys, as shown in Figure 2,[7] is dependent on their composition. For Al-Mg alloys that contain more than 1.5 pct of magnesium, loss of magnesium from the weld metal substantially increases hot crack susceptibility.

Experimental and theoretical investigations have been conducted to understand the vaporization of various species from the weld pool during fusion welding of several important engineering alloys and pure metals.[8–16] The weld metal composition change depends on the vaporization flux and the melting rate, the latter often being an important factor in determining the composition change.[17] In order to achieve a quantitative understanding of the vaporization and weld metal composition change, a comprehensive model is needed.

In early studies, the Langmuir equation[10,18] was widely used for the estimation of vaporization rates during welding. This simple model is useful in predicting the relative vaporization rates of various alloying elements. However, since it was derived for vaporization in vacuum, where no significant condensation of the vaporized species occurs, the Langmuir equation significantly overestimates the vaporization rate under commonly used welding conditions. For example, Sahoo *et al.*[11] found that at a pressure of 80 Pa (7.9×10^{-4} atm), the calculated vaporization rates of the pure metals obtained from the Langmuir equation were nearly one order of magnitude higher than the experimental results. Therefore, a realistic model for the calculation of the vaporization rate has to take into account the ambient pressure.

Anisimov and Rakhmatulina[19] and Knight[20] derived equations for the calculation of vaporization and condensation rates for pure metals by solving the equations of conservation of mass, momentum, and energy in a thin layer adjacent to the liquid-vapor interface, known as the Knudsen layer. Their results have been incorporated into several recent models[14,15,16] to calculate laser-induced vaporization rates and the resulting composition changes. Chan and Mazumdar[14] developed a one-dimensional model to calculate the laser-induced materials vaporization rates from molten aluminum, titanium, and a superalloy.

H. ZHAO, Graduate Assistant, and T. DEBROY, Professor, are with the Department of Materials Science and Engineering, The Pennsylvania State University, University Park, PA 16802.

Manuscript submitted June 8, 2000.

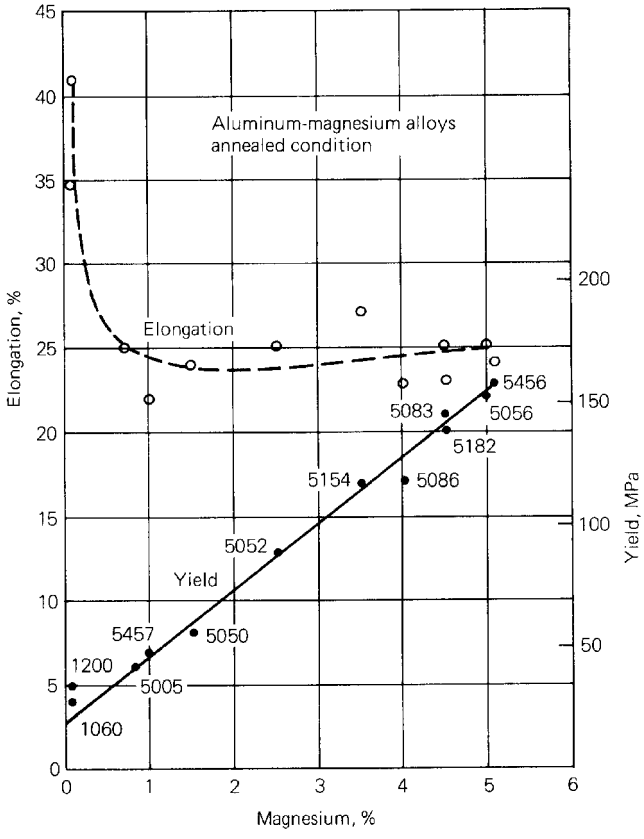

Fig. 1—Correlation between yield strength, elongation, and magnesium concentration for 5000 series aluminum alloys.[5]

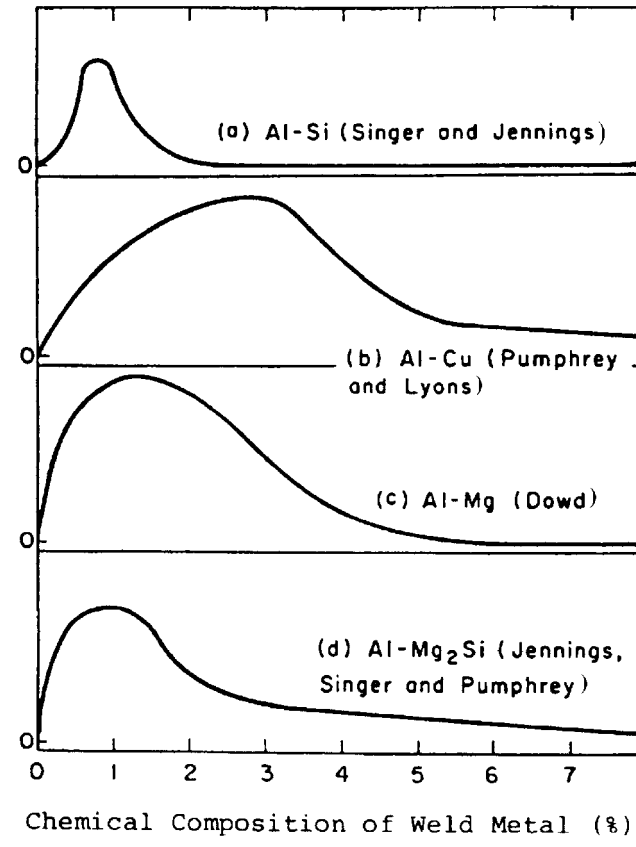

Fig. 2—(*a*) through (*d*) Effect of chemical composition of weld metal on relative crack susceptibility in various aluminum alloys.[7]

DebRoy *et al.*[15] and Mundra and DebRoy[16] coupled the principles of weld pool transport phenomena and vapor-phase gas dynamics for the calculation of the laser-induced vaporization of pure metals and stainless steel. Higher accuracy in the calculated vaporization rates was achieved due to the consideration of more details of the physical processes involved. However, the previous models[15,16] are two-dimensional and axisymmetric and therefore, they are applicable only to spot welding or to welding at low speeds. Furthermore, the application of these models was limited to steels and pure metals. No quantitative investigation on composition change during laser welding of automotive aluminum alloys has been reported in the literature so far.

The work presented in this article was conducted to understand quantitatively the influences of various welding variables on the vaporization rates and weld metal composition changes during conduction mode laser beam welding of automotive aluminum alloy 5182. A comprehensive model, integrating the calculation of turbulent fluid flow and heat transfer in three dimensions and the calculations of vaporization rate and composition change in the weld pool, was developed. Calculated weld pool geometry, vaporization rates, and composition changes were compared with the corresponding experimental results.

II. EXPERIMENTAL PROCEDURE

Bead-on-plate autogenous welds of aluminum alloy 5182 plates of 1-mm thickness were produced using a continuous wave Nd:YAG laser. The composition of the alloy is given in Table I. In the table, the concentrations of magnesium and zinc were determined by a spectrochemical technique from actual test samples while the concentrations of other elements are nominal specified values. The welding parameters used in this investigation are given in Table II. A defocused laser beam was used in order to obtain a conduction mode welding. A nomenclature of positive defocusing to represent the focal point to be above the top surface of the workpiece, and negative defocusing to represent the focal point to be below the top surface, will be used throughout this article. The laser beam was delivered using a 600-μm-diameter fiber of fused silica to an f2 focus optic manipulated by a micropositioning stage mounted on a linear translation device. An ancillary copper nozzle having an 8-mm inner diameter was utilized to provide helium shielding gas at a flow rate of 1.6 L/s.

Table I. Composition of Aluminum Alloy 5182

Alloying Element	Mg	Si	Mn	Cr	Cu	Zn	Ti	Al
Wt pct	4.20	0.20	0.35	0.10	0.15	0.07	0.10	balance

Table II. Welding Parameters Used in the Study

Laser power	1.5 to 3 kW
Welding speed	95.3 to 116.4 mm/s
Beam defocusing	±1.5, ±1.75, ±2 mm

After welding, the weld pool cross-sectional area, depth, and width were measured by standard metallography and computer image analysis. The elemental composition in the weld pool was determined by electron microprobe analysis. The concentrations of magnesium and aluminum in the weld metal were obtained from the average of at least 15 data points at different locations within the fusion zone. Since other alloying elements constitute less than 1 wt pct, they were not measured. In order to avoid erroneous data caused by localized interdendritic segregation, each elemental measurement was obtained over an area of $100 \times 100\ \mu m^2$.

MATHEMATICAL MODELING

A. *Heat Transfer and Fluid Flow in the Molten Pool*

The Navier–Stokes equations and the equation of conservation of energy were solved numerically to obtain the three-dimensional temperature and velocity fields in the weld pool. The standard K-ε turbulence model[21] was incorporated to calculate the effect of turbulent agitation in the weld pool. The transient problem was transformed into a steady state problem by the use of an Eulerian coordinate system. The heat loss due to the vaporization of alloying elements significantly influences the temperature field on the weld pool surface.[16] In the present model, the evaporative heat loss was taken into account in the boundary conditions on the pool surface. Since the appropriate equations and the boundary conditions have been well documented in the literature,[21–24] these are not presented here.

The power density distribution of the laser beam was Gaussian in nature. The distribution of absorbed laser power density on the weld pool surface is thus given by[25]

$$J(r) = \frac{2\eta Q}{\pi {r_b}^2}\, e^{(-2r^2/{r_b}^2)} \qquad [1]$$

where η is the absorption coefficient, Q is the laser power, r_b is the beam radius, and r is the radial distance from the beam axis. The beam radius at various locations along the beam axis z is given by[26]

$$r_b = r_0\,[\,1 + \{\lambda z M^2/(\pi {r_0}^2)\}]^{1/2} \qquad [2]$$

where r_0 is the beam radius at the focal point, λ is the beam wavelength, z is the beam defocusing, *i.e.*, the distance from the focal point to the top surface of the weldment, and M^2 is a dimensionless beam quality figure of merit that is given by[26]

$$M^2 = \pi r_0 \beta/\lambda \qquad [3]$$

where β is the half-angle of beam divergence. For a given laser, the value of M^2 usually varies with increasing laser power due to the intrinsic distortions of the laser beam.[26] For a Nd:YAG laser, intrinsic distortion is caused by the temperature gradient across the laser rod. As a result, the beam size often increases with increasing laser power. This effect is taken into account in the calculations.

B. *Composition Change in the Weld Pool*

The rate of vaporization for a metal is influenced by its equilibrium vapor pressure. The equilibrium vapor pressures of various alloying elements *vs* temperature are presented in Figure 3. It is observed that the vapor pressure of magnesium is much higher than that of aluminum and other elements, except zinc. Since the concentration of zinc in alloy 5182 is very low, only the vaporization of magnesium and aluminum were considered in the study.

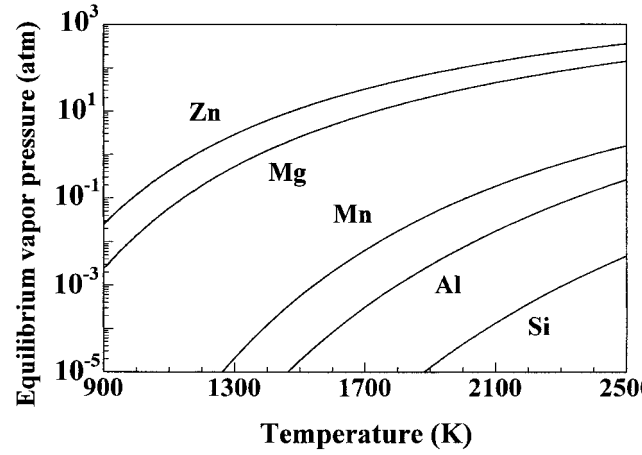

Fig. 3—Equilibrium vapor pressure of metals at different temperatures.

Several assumptions were made in the calculations: (1) the activity of magnesium in the molten pool was calculated assuming Henry's law,[27] *i.e.*, $a_{Mg} = 0.88 X_{Mg}$, while the activity of aluminum was obtained from Raoult's law, *i.e.*, $a_{Al} = X_{Al}$, where X_{Mg} and X_{Al} are the mole fraction of magnesium and aluminum in the alloy, respectively; and (2) the concentrations of aluminum and magnesium in the weld pool were considered to be uniform. This is justified owing to rapid mixing in the weld pool due to the vigorous convective flow of liquid metal.

1.1. *Vaporization flux*

a. Vapor flux due to concentration gradient

The concentrations of metal vapors are higher near the weld pool surface than in the bulk shielding gas. The vapor flux of element i, J_{ci}, due to such a concentration gradient is defined as

$$J_{c,i} = K_{g,i}\left(M_i \frac{a_i P_i^{o}}{RT_l} - C_i^{b}\right) \qquad [4]$$

where a_i is the activity of element i in the liquid metal, P_i^{o} is the equilibrium vapor pressure of element i over pure liquid, M_i is the molecular weight of element i, R is the gas constant, T_l is the temperature at the weld pool surface, $K_{g,i}$ is the mass transfer coefficient of element i, and C_i^{b} is the concentration of element i in the shielding gas. Since the concentration of element i in the shielding gas, C_i^{b}, is significantly lower than that at the weld pool surface, it can be neglected. The mass transfer coefficient between the weld pool surface and the exit of the shielding gas nozzle is calculated from the graphical results of Schlunder and Gniclinski for a jet impinging on a flat surface[28] and is given by

$$K_{g,i} = \frac{2\ \mathrm{Sc}_i^{0.42}\ \mathrm{Re}^{0.5}\ D_i}{d}\left(1 + \frac{\mathrm{Re}^{0.55}}{200}\right)^{0.5} \left[\,0.483 - 0.108\frac{r}{d} + 7.71 \times 10^{-3}\left(\frac{r}{d}\right)^2\right] \qquad [5]$$

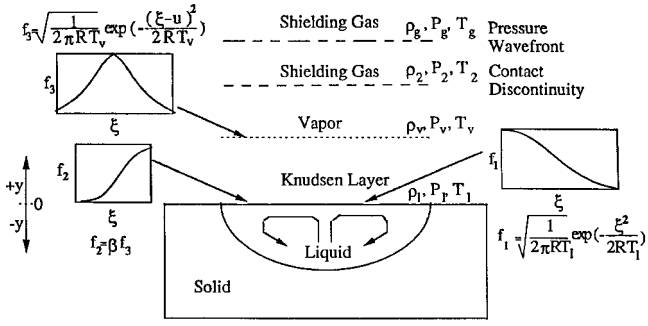

Fig. 4—Velocity distribution functions of vapor molecules at various locations.

where d is the diameter of the nozzle in meters, r is the radial distance on the pool surface in meters, D_i is the average diffusivity of element i in the shielding gas, Re is the Reynolds number at the nozzle exit, and Sc_i is the average Schmidt number.

b. *Vapor flux due to pressure gradient*

During laser welding, the peak temperature on the weld pool surface can exceed the boiling point of the alloy and, consequently, the vapor pressure at the weld pool surface can be higher than one atmosphere. For example, von Allmen[29] determined molten pool temperatures in excess of the boiling point for the laser treatment of copper. Batanov *et al.*[30] also indicated that temperatures on the surface of a laser-irradiated material can be higher than the boiling point. Chan and Mazumder[14] have also reported computed temperatures greater than the boiling point during laser irradiation of aluminum, titanium, and a superalloy. Theoretical calculations of the vaporization rates by Anisimov and Rakhmatulina[19] and Knight[20] are based on the premise that the liquid pool surface temperatures are higher than the boiling point. Therefore, the convective flux of the vaporized elements, driven by the excess pressure, is an important contributor to the overall vaporization flux.

The velocity distribution functions, f_1, f_2, and f_3 of the vapor molecules escaping from the weld pool surface at various locations are shown schematically Figure 4. On the weld pool surface, the velocity distribution, f_1, is half-Maxwellian because the vapor molecules only move away from the pool surface, *i.e.* the velocity varies from 0 to $+\infty$. There exists a space of several mean free paths length near the weld pool surface, known as the Knudsen layer, at the outer edge of which the velocity distribution, f_3, just reaches Maxwellian. Here, the velocity can vary from $-\infty$ to $+\infty$, as shown in Figure 4. A portion of the vaporized material, f_2, condenses on the liquid surface. This rate of condensation was taken into account in the model.

The temperature T_v, density ρ_v, pressure P_v, and the mean velocity u of the vapor at the edge of the Knudsen layer can be related to temperature T_l, density ρ_l, and pressure P_l of the vapor at the liquid surface by treating the Knudsen layer as a gas dynamic discontinuity. Anisimov and Rakhmatulina[19] and Knight[20] derived expressions for the jump conditions in the vapor temperature, density, velocity, and the extent of condensation across the Knudsen layer by solving the equations of the conservation of mass, momentum, and translational kinetic energy, using the velocity distribution functions presented in Figure 4. The derived jump conditions across the Knudsen layer are given by

$$\frac{T_v}{T_l} = \left[\sqrt{1 + \pi\left(\frac{\gamma_v - 1}{\gamma_v + 1}\frac{m}{2}\right)^2} - \sqrt{\pi}\,\frac{\gamma_v - 1}{\gamma_v + 1}\frac{m}{2}\right]^2 \quad [6]$$

$$\frac{\rho_v}{\rho_l} = \sqrt{\frac{T_l}{T_v}}\left[\left(m^2 + \frac{1}{2}\right)e^{m^2}\,\mathrm{erfc}\,(m) - \frac{m}{\sqrt{\pi}}\right] + \frac{1}{2}\frac{T_l}{T_v}\left[1 - \sqrt{\pi}me^{m^2}\,\mathrm{erfc}\,(m)\right] \quad [7]$$

$$\beta = \left[(2m^2 + 1) - m\sqrt{\pi\frac{T_l}{T_v}}\right]e^{m^2}\frac{\rho_l}{\rho_v}\sqrt{\frac{T_l}{T_v}} \quad [8]$$

where $m = u/\sqrt{2R_vT_v}$, R_v, $= R/M_v$, R is the gas constant, γ_v, is the ratio of specific heats of the vapor, which is treated as a monatomic gas, and β is the condensation factor. The equilibrium vapor pressure P_l, at the pool surface is obtained from the equilibrium vapor pressure-temperature relationships of the various alloying elements:

$$P_l = \sum_{i=1}^{n} a_i P_i^\circ \quad [9]$$

and M_v, the average molecular weight of the vapor, is given by

$$M_v = \sum_{i=1}^{n} M_i\frac{a_iP_i^\circ}{P_l} \quad [10]$$

where a_i the activity of element i in the weld pool, P_i° is the equilibrium vapor pressure of pure element i at temperature T_l, and M_i is the molecular weight of element i.

There are four unknowns in eqs. [6] through [8], namely, T_v, ρ_v, β, and m. Therefore, another independent equation is required to obtain the unique values of these variables. The necessary equation is obtained by applying the Rankine–Hugoniot relation[31] to relate the pressure at the edge of the Knudsen layer to the ambient conditions by

$$\frac{P_l}{P_g}\frac{P_2}{P_l} = 1 + \gamma_g\,\mathrm{M}\Gamma\left[\frac{\gamma_g + 1}{4}\mathrm{M}\Gamma + \sqrt{1 + \left(\frac{\gamma_g + 1}{4}\mathrm{M}\Gamma\right)^2}\right] \quad [11]$$

where P_g and P_2 are the pressures in front of and behind the wavefront, respectively, $P_2 = P_v$, γ_g is the ratio of specific heats for shielding gas, $\Gamma = \sqrt{\gamma_vR_vT_v}/\sqrt{\gamma_gR_gT_g}$, and M is the Mach number which is related to m by the relation

$$m = \mathrm{M}\sqrt{\frac{\gamma_v}{2}} \quad [12]$$

The Mach number M and the density ρ_v, obtained by solving Eqs. [6] through [12], can be used to calculate the vaporization flux due to pressure gradient at the weld pool surface corresponding to a local surface temperature T_l from

$$J_P = \rho_v\mathrm{M}S \quad [13]$$

where S is the speed of sound in vapor at temperature T_v. The vaporization flux of an alloying element i, J_{Pi}, is given by the product of the total vapor flux and the mole fraction of i in the gas

Table III. Data Used for the Calculations of Weld Pool Temperature and Velocity Fields[5,32–34]

Property (Unit)	Value	Reference
Liquidus temperature (K)	911	32
Solidus temperature (K)	850	32
Density of liquid metal (kg/m^3)	2300	5
Enthalpy of solid at melting point (J/g)	721	5
Enthalpy of liquid at melting point (J/g)	1116	5
Specific heat of solid (J/g K)	0.9	5
Specific heat of liquid (J/g K)	1.2	5
Thermal conductivity of solid (J/m s K)	168	5
Thermal conductivity of liquid (J/m s K)	108	5
Viscosity of liquid (g/m s)	1.1	5
Temperature coefficient of surface tension (N/m K)	-3.5×10^{-4}	33
Heat of vaporization for Mg (J/g)	5253	33
Heat of vaporization for Al (J/g)	10,780	33
Partial heat of mixing for Mg in Al (J/g)	556	34

$$J_{P,\mathrm{i}} = a_{\mathrm{i}} \frac{P_{\mathrm{i}}^{\circ}}{P_{\mathrm{l}}} \frac{\mathrm{M}_i}{\mathrm{M}_v} J_P \qquad [14]$$

From the results of Eqs. [4] and [14], the total vaporization flux for element i can be obtained from

$$J_{\mathrm{i}} = J_{c,\mathrm{i}} + J_{P,\mathrm{i}} \qquad [15]$$

2. *Vaporization rate and composition change*

The vaporization rate of element i, G_{i} is obtained by integrating the vapor flux over the entire weld pool surface, and the total vaporization rate of all the elements, G, is given by

$$G = \sum_{\mathrm{i}=1}^{n} G_{\mathrm{i}} = \sum_{\mathrm{i}=1}^{n} \iint_{s} J_{\mathrm{i}}\, dx\, dy \qquad [16]$$

where J_{i} is the vapor flux of element i and s indicates the weld pool surface. The final composition in the weld pool is calculated by an iterative scheme with the initial values chosen to be those of the base metal. The concentration of element i in the weld pool, C_i, is given by

$$C_{\mathrm{i}} = \frac{\nu A \rho C_{\mathrm{i},b} - G_{\mathrm{i}}}{\nu A \rho - G} \qquad [17]$$

where C_{i} and $C_{\mathrm{i},b}$ are the concentration of element i in the weld pool and in the base metal, respectively, ν is the welding speed, A is the across section area of the weld, and ρ is the density of the weld metal. After each iteration, the activities of the alloying elements in the weld pool are recalculated based on the calculated composition in the weld pool. Using the new values of activities of alloying elements, all calculations are repeated until the calculated composition in the weld pool converges.

C. *Data Used in the Calculations*

The temperature and velocity fields in the weld pool were calculated using the data presented in Table III.[5,32–34] The surface condition and the addition of alloying elements greatly affects the absorption of laser radiation by aluminum. The reported values of the absorption coefficient of Nd:YAG laser radiation by aluminum alloys vary from about 0.05 for very clean aluminum[35,36] to about 0.45 for chemically etched alloy AA1050.[37] Due to the high sensitivity of the absorption coefficient to the surface conditions, small variations in absorption coefficient are expected. In the present model, the absorption coefficient was adjusted in the range of 0.22 to 0.25 to fit the experimentally determined weld pool size.

Table IV. Welding Conditions and the Corresponding Beam Radius and Absorption Coefficient Used for the Calculations

Nominal Power (W)	Measured Power (W)	Beam Defocusing (mm)	Welding Speed (mm/s)	Absorption Coefficient	Beam Radius (mm)
1500	1600	1.50	105.8	0.23	0.32
2000	1700	1.50	105.8	0.25	0.35
2500	2040	1.50	105.8	0.23	0.38
3000	2510	1.50	105.8	0.22	0.41
3000	2510	1.75	95.3	0.22	0.42
3000	2510	1.75	105.8	0.22	0.42
3000	2510	1.75	116.4	0.22	0.42
3000	2510	2.00	95.3	0.23	0.43
3000	2510	2.00	105.8	0.23	0.43
3000	2510	2.00	116.4	0.23	0.43

The laser beam radius and absorption coefficient for various welding conditions are presented in Table IV. The nominal laser powers, which are different from the measured laser powers, are used to identify the welding conditions throughout this article. The data used for the calculation of vapor fluxes are presented as a function of temperature T and/or pressure P, as shown in Table V.[33,38]

IV. RESULTS AND DISCUSSION

A. *Temperature and Velocity Fields in the Weld Pool*

The calculated temperature and velocity fields in weld pool cross sections and the experimentally obtained weld pools for laser powers of 1.5 and 3 kW are shown in Figure 5. It is observed that the calculated weld pool geometry and dimensions agree well with the experimental results. The peak temperatures near the center of the weld pool were about 2150 K, and these decreased progressively toward the periphery. For both cases, there is a recirculating flow in the weld pool driven mainly by surface tension (Marangoni) force. Since the temperature coefficient of surface tension is negative for this alloy, the molten metal on the surface flows from the center to the periphery of the pool, as shown in Figure 5. The maximum flow velocities on the weld pool surface are on the order of 1 m/s. The general features of the calculated temperature and velocity fields are consistent with the calculated results reported in the literature.[22–24,39]

The high velocity flows occurring in weld pools resulted in rapid mixing and caused turbulence, which enhanced the rates of transport of energy and momentum. In the present model, turbulence was simulated by the use of effective viscosity, $\mu_{\mathrm{eff}} = \mu + \mu_t$, and effective thermal conductivity, $k_{\mathrm{eff}} = k + k_t$, in the equations of conservation of energy

Table V. Data Used for the Calculations of Vaporization Rates[33,38]

Parameter	Formula	Reference
Viscosity of He (g/m s)	$2.20 \times 10^{-2} + 2.22 \times 10^{-5} \times T$	38
Diffusivity of Al in He (mm^2/s)	$(-1.20 \times 10^2 + 0.39 \times T + 2.09 \times 10^{-4} \times T^2)/P$	38
Diffusivity of Mg in He (mm^2/s)	$(-1.10 \times 10^{-2} + 0.36 \times T + 1.96 \times 10^{-4} \times T^2)/P$	38
Al vapor pressure, P (atm)	$\log P = 12.36 - 1.65 \times 10^4/T - 1.02 \times \log T - \log 760$	33
Mg vapor pressure, P (atm)	$\log P = 12.79 - 7.55 \times 10^3/T - 1.41 \times \log T - \log 760$	33

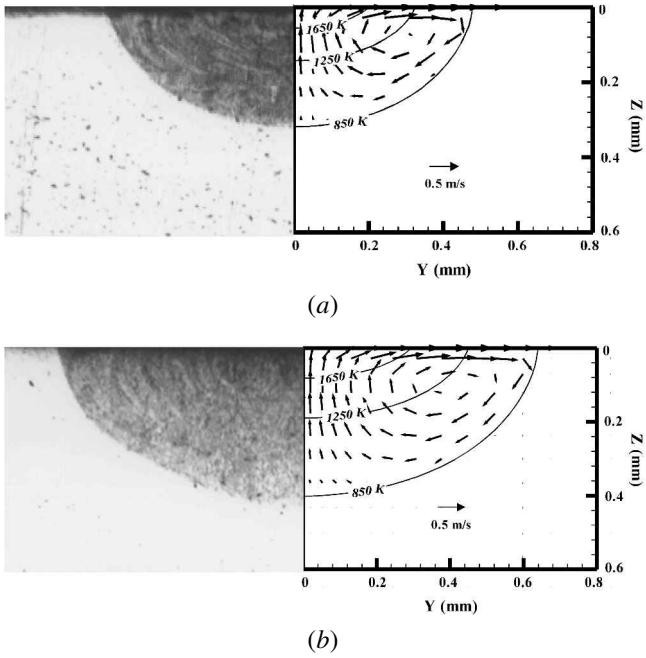

Fig. 5—Experimental and calculated weld pool cross sections for laser power of (*a*) 1.5 kW and (*b*) 3.0 kW. Welding speed 105.8 mm/s and beam defocusing +1.5 mm.

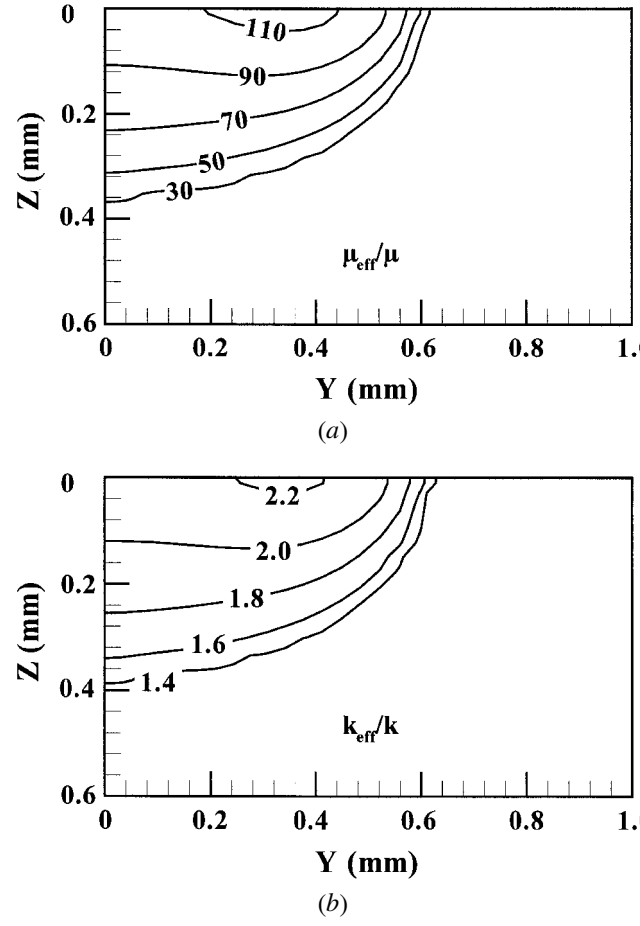

Fig. 6—Distributions of (*a*) ratio of effective to molecular viscosity and (*b*) ratio of effective to molecular thermal conductivity in weld pool cross section. Laser power 3 kW, welding speed 105.8 mm/s, and beam defocusing ±1.5 mm.

and momentum. Here, μ and k are the molecular values of viscosity and thermal conductivity of the liquid, respectively. The turbulent viscosity μ_t and turbulent thermal conductivity k_t in the weld pool were calculated by solving the equations of conservation of turbulent kinetic energy K and its dissipation rate ε from the K-ε model.

The distributions of the ratio of effective to molecular viscosity, μ_{eff}/μ, and the ratio of effective to molecular thermal conductivity, k_{eff}/k, in the cross section of a weld pool are shown in Figure 6. The ratio of turbulent to molecular viscosity, μ_t/μ, reflects the degree of turbulence and is also defined as turbulence Reynolds number. The flow is considered fully turbulent when the value of μ_t/μ is higher than 100.[39] Figure 6(a) shows that the maximum value of μ_t/μ is more than 110 near the weld pool surface, indicating a fully turbulent flow there. The maximum value of μ_t/μ is almost the same as that obtained for gas-tungsten-arc (GTA) welding of aluminum alloy 6061.[39] The distribution of the ratio of effective to molecular thermal conductivity, k_{eff}/k, shown in Figure 6(b) has the same pattern as that of μ_{eff}/μ. The maximum value of k_{eff}/k is about 2.5. It is observed that the maximum values of μ_t/μ and k_t/k occur at locations where the velocity gradient is the highest. The values and distribution patterns of μ_{eff}/μ and k_{eff}/k shown in Figure 6 are comparable with results in the literature.[39]

B. *Vaporization and Composition Change*

The distributions of temperature and various vapor fluxes on the weld pool surface are shown in Figure 7. The total vapor flux is the sum of fluxes in parts (b) and (c) or alternatively, the sum of fluxes in parts (d) and (e). It is observed that the distribution patterns of vapor fluxes are similar to the patterns of the surface temperature, indicating the vapor fluxes are predominantly determined by temperature. Most of the vaporization occurs from a small region near the center of the beam-workpiece interaction zone where the weld pool surface temperatures exceed the boiling point of the alloy (about 1930 K). The vaporization flux here is primarily driven by the pressure gradient. The radius of this active region is approximately 0.15 mm, which is

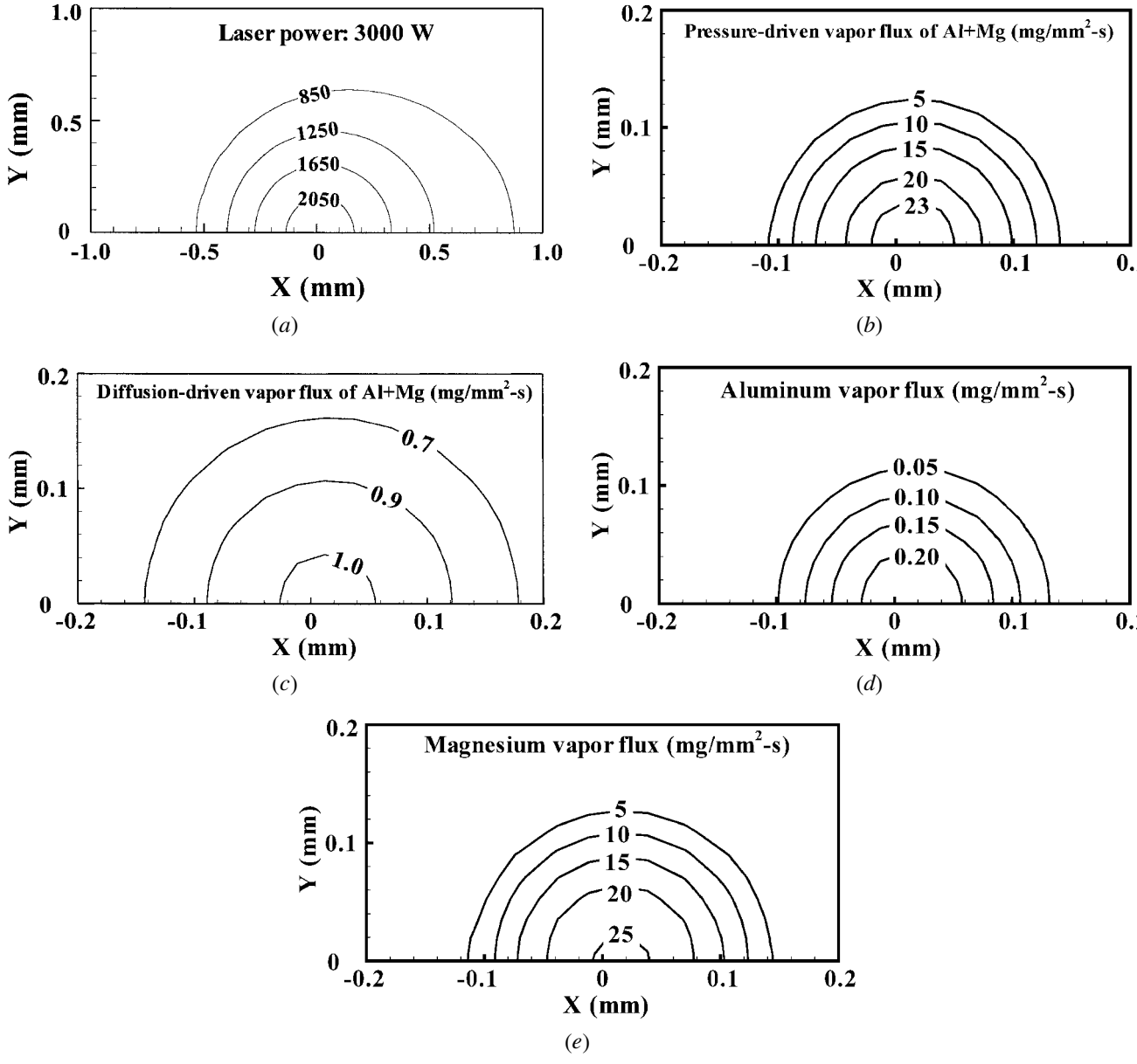

Fig. 7—(*a*) through (*e*) Distributions of temperature and various vapor fluxes on the weld pool surface. Laser power 3 kW, welding speed 105.8 mm/s, and beam defocusing ±1.5 mm.

smaller than the laser beam radius of 0.41 mm. The vaporization flux outside of this active region is very low and is driven by diffusion. Figure 7 also shows that magnesium vapor flux is about two orders of magnitude greater than aluminum vapor flux, resulting in a lowering of the magnesium concentration in the weld metal.

The vaporization rates of alloying elements were calculated by integrating the vapor fluxes over the weld pool surface in the model. The vaporization rates can also be obtained from the experimental data of magnesium loss from the weld pool ΔC_{Mg}, the weld pool cross section area A, and the welding speed ν. Assuming the vaporization rate of aluminum to be negligible, a mass balance of magnesium results in the following expression for magnesium vaporization rate G_{Mg}:

$$G_{Mg} = \Delta C_{Mg}\, \rho \nu A \qquad [18]$$

where ρ is the density of the alloy. The experimental data of magnesium loss in the weld pool ΔC_{Mg} were obtained from the concentration profiles across the weld pool, as shown in Figure 8.

The computed vaporization rates are compared with the corresponding experimental values in Table VI. The data show that the calculated rates agree well with the experimental results for various welding conditions. Therefore, the comprehensive modeling presented here can serve as a basis for the quantitative understanding of the influences of various welding parameters on weld pool geometry, vaporization rate, and composition change during conduction mode laser welding of aluminum alloys.

C. *Influence of Laser Power*

According to eq. [18], the composition change from evaporation during welding is proportional to the ratio of vaporization rate and melting rate given by $\rho \nu A$. At a constant

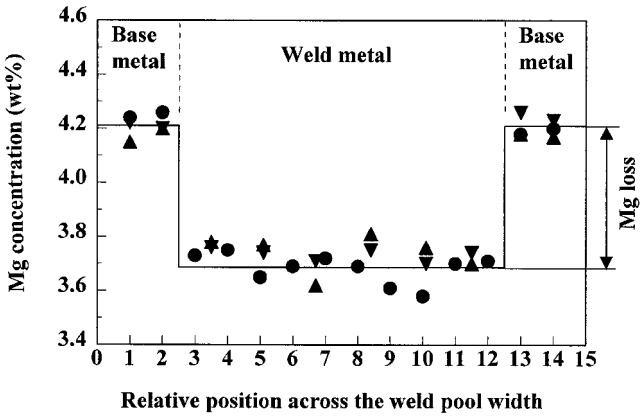

Fig. 8—Typical magnesium concentration profile across the weld pool width. The data were taken on three weld pool cross sections made using the same welding conditions: laser power 3 kW, welding speed 105.8 mm/s, and beam defocusing +1.5 mm.

welding speed, the melting rate is proportional to the cross sectional area *A*. The influences of laser power on weld pool cross-sectional area, vaporization rate, and composition change in the weld pool are presented in Figure 9. Data in Figure 9(a) show that both the vaporization rate and the cross-sectional area increased roughly equally with the increase in the power, and kept their ratio almost constant. Since this ratio was not sensitive to laser power, the difference in the concentrations of magnesium between the base metal and the weld metal was not affected by the laser power. This behavior is observed in Figure 9(b).

It is instructive to compare the observed effect of power on the compositional change in the aluminum alloy with that reported for loss of manganese from stainless steels during laser welding. During CO_2 laser welding of stainless steel,[12] the change in the weld pool size with power was much more pronounced than that for the aluminum alloy. As a result, the change in the concentration of manganese was much more pronounced at low powers. Therefore, the quantitative understanding of the influences of laser power

Table VIa. Calculated and Experimental Weld Pool Geometry, Vaporization Rate, and Loss of Magnesium in the Weld Pool for Different Laser Powers at Welding Speed of 105.8 mm/s and Beam Defocusing of ±1.5 mm

Laser power (W)	1500		2000	
Calculated or experimental	Calculated	Experiment	Calculated	Experiment
Depth (mm)	0.32	0.31	0.35	0.35
Width (mm)	0.96	0.98	1.06	1.04
Cross-sectional area (mm^2)	0.24	0.23	0.29	0.29
Vaporization rate (mg/s)	0.32	0.32	0.45	0.44
Δwt pct Mg loss	0.47	0.49	0.54	0.55
Laser power (W)	2500		3000	
Calculated or experimental	Calculated	Experiment	Calculated	Experiment
Depth (mm)	0.36	0.37	0.40	0.42
Width (mm)	1.12	1.11	1.26	1.32
Cross-sectional area (mm^2)	0.32	0.31	0.39	0.40
Vaporization rate (mg/s)	0.53	0.49	0.59	0.58
Δwt pct Mg loss	0.56	0.57	0.53	0.52

Table VIb. Calculated and Experimental Weld Pool Geometry, Vaporization Rate, and Loss of Magnesium in the Weld Pool for Different Welding Speed and Beam Defocusing at Laser Power of 3 kW

Beam defocusing (mm)	±1.75					
Welding speed (mm/s)	95.3		105.8		116.4	
	Calculated	Experiment	Calculated	Experiment	Calculated	Experiment
Depth (mm)	0.41	0.41	0.40	0.41	0.39	0.37
Width (mm)	1.27	1.26	1.26	1.27	1.20	1.20
Cross section area (mm^2)	0.40	0.39	0.39	0.39	0.35	0.34
Vaporization rate (mg/s)	0.69	0.64	0.72	0.60	0.68	0.59
Δwt pct Mg loss	0.66	0.65	0.64	0.55	0.61	0.56
Beam Defocusing (mm)	±2.00					
Welding speed (mm/s)	95.3		105.8		116.4	
	Calculated	Experiment	Calculated	Experiment	Calculated	Experiment
Depth (mm)	0.42	0.44	0.42	0.42	0.40	0.40
Width (mm)	1.33	1.35	1.30	1.29	1.25	1.26
Cross section area (mm^2)	0.43	0.46	0.41	0.41	0.39	0.38
Vaporization rate (mg/s)	0.68	0.68	0.69	0.76	0.69	0.70
Δwt pct Mg loss	0.60	0.59	0.57	0.66	0.55	0.60

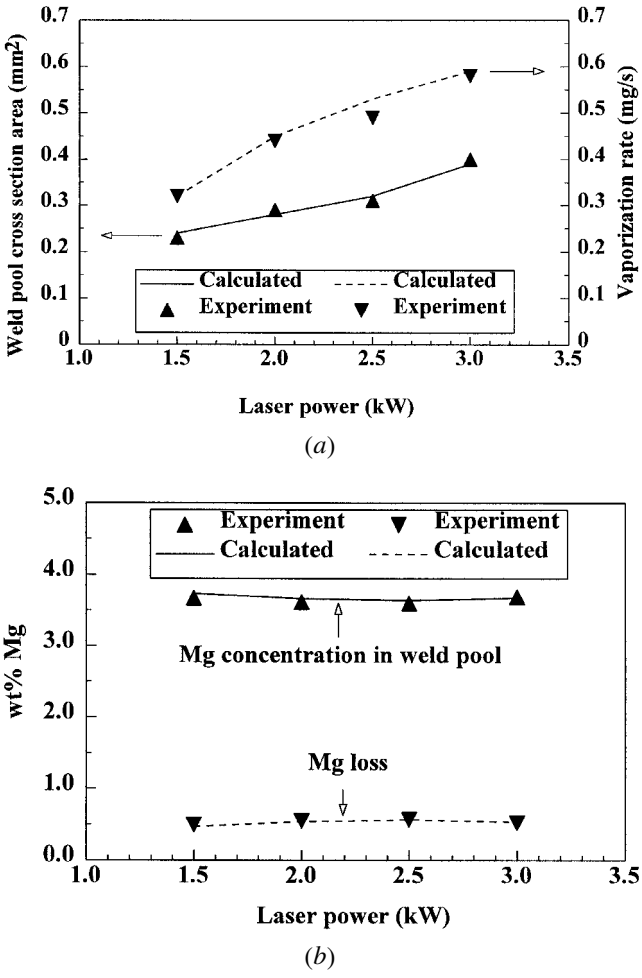

Fig. 9—(*a*) and (*b*) Influence of laser power on weld pool size, vaporization rate, and composition change. Welding speed 105.8 mm/s and beam defocusing ±1.5 mm.

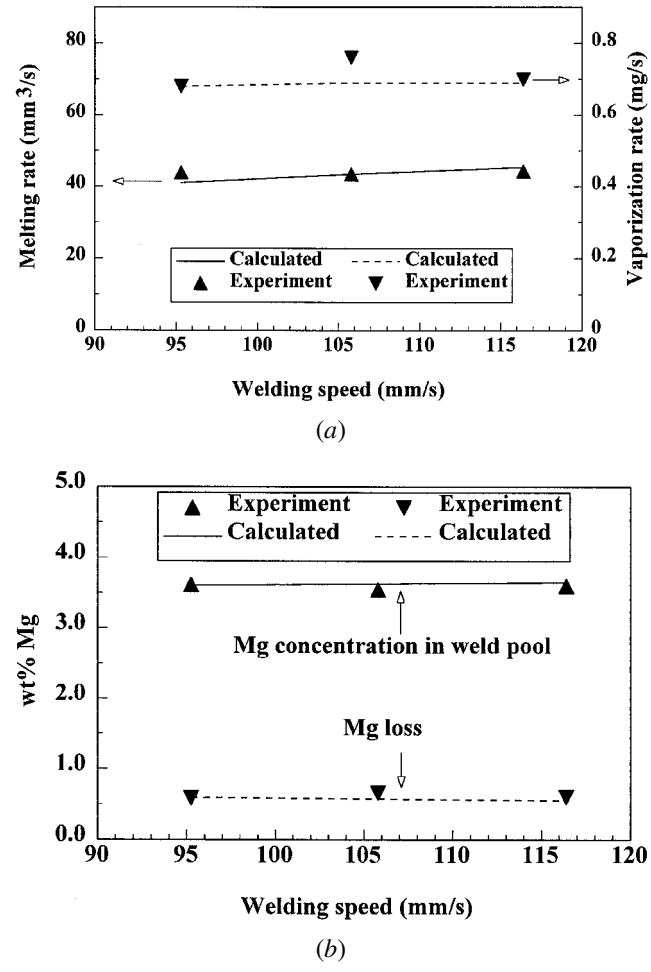

Fig. 10—(*a*) and (*b*) Influence of welding speed on melting rate, vaporization rate, and composition change. Laser powers 3 kW and beam defocusing ±2 mm.

on weld pool cross-sectional area and vaporization rate is a key in predicting weld metal composition change for welding with different laser powers.

D. *Influence of Welding Speed*

The influence of welding speed on the melting rate, vaporization rate, and composition change are presented in Figure 10. The decrease in weld pool cross section area was roughly compensated by the increase in welding speed and, as a result, the melting rate did not change significantly with welding speed, as shown in Figure 10(a). Similarly, the vaporization rate was almost unaffected by the welding speed in the range of variables reported in this investigation. Since the ratio of the vaporization rate and the melting rate was almost constant, the difference in the concentration of magnesium between the base metal and the weld metal did not vary with welding speed, as shown in Figure 10(b).

A similar result was also reported by Khan *et al.*,[12] who, for a different reason, found that the composition change during the CO_2 laser welding of stainless steels was not sensitive to welding speed. Unlike in the welding of aluminum alloys using a Nd:YAG laser, in the CO_2 laser welding of stainless steels, absorption of the laser beam by plasma was important and as a result, beam absorption by the workpiece was more efficient at higher welding speeds. Consequently, the vaporization rate of manganese increased somewhat with the increase in welding speed. However, this increase was compensated for by the increase in the product of the weld pool cross-sectional area and the welding speed, *i.e.*, the volumetric melting rate. Therefore, the composition change in the welding of stainless steel and aluminum alloy 5182 was practically unaffected by the changes in the welding speed.

V. SUMMARY AND CONCLUSIONS

The weld metal composition change during conduction mode continuous wave laser beam welding of aluminum alloy 5182 was investigated through experiments and computer modeling. The major findings are as follows:

1. The vaporization rate of magnesium was about two orders of magnitude greater than that of aluminum. The significant magnesium loss from the weld pool resulted in a lower magnesium concentration in the weld metal than was present in the base metal. The vaporization rate increased with an increase in laser power. However, the higher loss was compensated for by an equivalent

increase in the melting rate and, as a result, the concentration of magnesium in the weld metal, although lower than that found in the base metal, was not affected by changes in the laser power. The weld metal composition was also unaffected by the variation of welding speed for the welding conditions investigated in this research.
2. Calculations showed that for all the welding conditions studied here, the peak temperature at the weld pool surface slightly exceeded the boiling point of the alloy. As a result, the pressure in a small region near the center of the weld pool surface was higher than one atmosphere. Vaporization was most pronounced in this active region, which had a smaller cross-sectional area than the laser beam. The vaporization here was predominantly driven by the pressure gradient that existed between the weld pool surface and the atmosphere. The vaporization rate outside of the active region was much lower.
3. A comprehensive model for the calculation of temperature and velocity fields, vaporization rates, and weld metal composition changes during conduction mode laser welding was developed. The calculated results of weld pool geometry, vaporization rates, and composition changes agreed well with the corresponding experimental results. The extent of the agreement between the calculated and experimental results indicates that the model can serve as a basis for the quantitative understanding of influences of various welding parameters on fluid flow and heat transfer, vaporization of alloying elements, and weld metal composition changes during laser welding.

ACKNOWLEDGMENTS

Financial support for this work was provided by the United States Department of Energy (Grant No. DE-FG02-96ER45602).

REFERENCES

1. L. Griffing: *Welding Handbook*, Sec. 4, *Metals and Their Weldability*, American Welding Society, Miami, FL, 1972.
2. P.A. Hilton: *Optical and Quantum Electronics,* 1995, vol. 27, pp. 1127-47.
3. B. Irving: *Welding J.*, 1991, vol. 71 (9), pp. 39-45.
4. H. Zhao, D. White, and T. DebRoy: *Int. Mater. Rev.*, 1999, vol. 44 (6), pp. 238-66.
5. J.E. Hatch: *Aluminum: Properties and Physical Metallurgy*, American Society for Metals, Metals Park, OH, 1984.
6. M.J. Cieslak and P.W. Fuerschbach: *Metall. Trans.*, 1988, vol. 19B, pp. 319-29.
7. J.H. Dudas and F.R. Collins: *Welding J.*, 1966, vol. 45, pp. 241s-249s.
8. A. Block-Bolten and T.W. Eagar: *Metall. Trans. B*, 1984, vol. 15B, pp. 461-69.
9. M.M. Collur, A. Paul, and T. DebRoy: *Metall. Trans. B*, 1987, vol. 18B, pp. 733-40.
10. P.A.A. Khan and T. DebRoy: *Metall. Trans. B*, 1984, vol. 15B, pp. 641-44.
11. P. Sahoo, M.M. Collur, and T. DebRoy: *Metall. Trans. B*, 1988, vol. 19B, pp. 967-72.
12. P.A.A. Khan, T. DebRoy, and S.A. David: *Welding J.*, 1988, vol. 67, pp. 1s-7s.
13. M. Pastor, H. Zhao, R.P. Martukanitz, and T. DebRoy: *Welding J.*, 1999, vol. 78, pp. 207s-16s.
14. C.L. Chan and J. Mazumder: *J. Appl. Phys.*, 1987, vol. 62, pp. 4579-586.
15. T. DebRoy, S. Basu, and K. Mundra: *J. Appl. Phys.*, 1991, vol. 70, pp. 1313-19.
16. K. Mundra and T. DebRoy: *Metall. Trans. B*, 1993, vol. 24B, pp. 145-55.
17. S.A. David and T. DebRoy: *Science*, 1992, vol. 257, pp. 497-502.
18. S. Dushman and J.M. Lafferty: *Scientific Foundations of Vacuum Science*, 2nd ed., John Wiley, New York, NY, 1962, pp. 15-21.
19. S.I. Anisimov and A.K. Rakhmatulina: *Soviet Physics-JET*, 1973, vol. 37, pp. 441-44.
20. C.J. Knight: *AIAA J.*, 1979, vol. 17, pp. 519-23.
21. B.E. Launder and D.B. Spalding: *Mathematical Models of Turbulence*, Academic Press, New York, NY, 1972.
22. Z. Yang, J.W. Elmer, J. Wong, and T. DebRoy: *Welding J.*, 2000, vol. 79, pp. 97s-112s.
23. S. Kou and Y.H. Wang: *Metall. Trans. A*, 1986, vol. 17A, pp. 2265-70.
24. G.M. Oreper and J. Szekely: *J. Fluid Mech.*, 1984, vol. 147, pp. 53-79.
25. P. Mouroulis and J. Macdonald: *Geometrical Optics and Optical Design*, Oxford University Press, Cambridge, United Kingdom, 1997, p. 302.
26. K.D. Hachfeld: in *The Industrial Laser Handbook*, D. Belforte and M. Levitt, eds., Springer-Verlag, New York, NY, 1992–93 pp. 48-54.
27. B.L. Tiwari: *Metall. Trans. A*, 1987, vol. 18A, pp. 1645-51.
28. E.U. Schlunder and V. Gniclinski: *Chem.-Ing.-Technol.*, 1967, vol. 39, pp. 578-84.
29. M. von Allmen: *Laser-Beam Interactions with Materials*, Springer-Verlag, Berlin, 1987.
30. V.A. Batanov, F.V. Bunkin, A.M. Prokhorov, and V.B. Fedorov: *Sov. Phys.-JETP*, 1973, vol. 36, pp. 311-22.
31. W.G. Vincenti and C.H. Kruger, Jr.: *Introduction to Physical Gas Dynamics*, Wiley, New York, NY, 1965.
32. *ASM Handbook*, vol. 2, *Properties and Selection—Nonferrous Alloys and Special-Purpose Materials*, 10th ed., ASM INTERNATIONAL, Materials Park, OH, 1990.
33. E.A. Brandes: *Smithells Metals Reference Book*, 6th ed., in association with Fulmer Research Institute Ltd., Butterworth and Co., London, 1983.
34. R. Hultgren: *Selected Values of Thermodynamic Properties of Metals and Alloys*, ASM, Metals Park, OH, 1973.
35. W.T. Walter, N. Solimene, K. Park, T.H. Kim, and K. Mukherjee: in *Laser in Metallurgy*, K. Mukherjee and J. Mazumder, eds., TMS-AIME, 1981, pp. 179-94.
36. W.W. Duley: in *Laser Surface Treatment of Metals*, C.W. Draper and P. Mazzoldi, eds., Kluwer Academic Publishers, Hingham, MA, 1986, pp. 3-15.
37. T. Watanabe, Y. Yoshida, and T. Arai: *LAMP'92*, Japan High Temperature Society, Nagaoka, 1992, pp. 505-10.
38. K. Mundra: Ph.D. Thesis, The Pennsylvania State University, University Park, PA, 1994.
39. D.C. Weckman: in *Trends in Welding Research (USA)*, J.M. Vitek, S.A. David, J.A. Johnson, H.B. Smartt, and T. DebRoy, eds., ASM INTERNATIONAL, Materials Park, OH, 1998, pp. 3-12.